CHAPTER IV

HYDROXYAPATITE/OVALBUMIN COMPOSITE PARTICLES AS MODEL PROTEIN CARRIERS FOR BONE TISSUE ENGINEERING: I. SYNTHESIS AND CHARACTERIZATION

4.1 Abstract

Hydroxyapatite (HAp) nanoparticles were synthesized from the co-precipitation reaction between calcium oxide from discarded egg shells and phosphoric acid in the absence and the presence of egg ovalbumin (OVA). 2-Amino-2-hydroxymethyl-propane-1,3-diol (tris- base) was used to control the pH during the co-precipitation (i.e., 7-9). The formation of HAp was confirmed by X-ray diffraction analysis, while both the Fourier-transform infrared spectroscopy and the thermogravimetric analysis confirmed the existence of OVA within the HAp/OVA composite particles. The crystallite sizes of the individual crystalline entities within the HAp and the HAp/OVA composite particles were approximated from the Scherrer's equation from the (002) reflection peak. The average particle sizes of the HAp and the HAp/OVA composite particles were measured by particle size analysis. Transmission electron microscopy revealed that these particles were aggregates of rod-like HAp nanocrystals, whereas the agglomeration of these particles into larger aggregates was revealed by scanning electron microscopy. Lastly, the decrease in the pH during the precipitation process and the presence of OVA were responsible for the observed increase in the values of pore size, BET specific surface area, and pore volume of the resulting HAp particles.

(**Key-words**: Hydroxyapatite; Ovalbumin; Composite particles)

4.2 Introduction

Hydroxyapatite (HAp), the major inorganic composition of hard bone tissues, is usually fabricated or imparted into prosthetic devices for bone implantation/replacement. This is because of its high biocompatibility and good

osteoconductivity (Kuriakose, 2004; Djošic, 2008; Ioku, 2009). Recently, porous HAp particles with pore size of 2-50 nm (mesoporous) or <2 nm (microporous) are found to be highly suitable for biomedical applications, especially for bone tissue engineering (Shanthi, 2010; Fischer, 2003). Mesoporous HAp particles having high surface areas and large pore volumes can be excellent carriers for delivery of functional biomolecules (Tjandra *et al.*, 2008). Such HAp particles can be prepared by many approaches, e.g., hydrothermal (Ioku *et al.*, 2009), emulsion (Bose *et al.*, 2003), sol-gel (Kuriakose, 2004; Bose, 2003), and precipitation (Viswanath, 2008; Wang, 2008) means. They can also be synthesized from many types of chemical templates, such as cationic surfactants, e.g., cetyltrimethylammonium bromide (CTAB) (Li, 2008; Wang, 2008; Wang, 2006), non-ionic surfactants, e.g., a triblock copolymer (Zhau *et al.*, 2005), and anionic surfactants, e.g., dodecyl phosphate (Wu *et al.*, 2005). The chemical templating technique poses some disadvantages, however. These are, for example, the deterioration of the mesopores (Li *et al.*, 2008) and the significant difference of the pore sizes (Wang *et al.*, 2008) after calcination. Biosurfactants can also be used to prepare mesoporous apatitic materials, because of their non-toxicity, low production cost, and the possibility of imparting relatively large pore sizes (>5 nm). Among the various biosurfactants, ovalbumin is very interesting, because of its abundance, cheapness, and being able to form cross-linked structures that are highly hydrated and porous-like (Zhao *et al.*, 2008).

In the present contribution, we proposed an environmentally friendly strategy towards the synthesis of protein-incorporated mesoporous hydroxyapatite (HAp) composite particles, using egg shells and egg ovalbumin (OVA) as raw materials. In addition to the use of OVA to enlarge the mesoporous structure to the obtained HAp particles, it was also used as the model, incorporating protein.

4.3 Experimental

4.3.1 Materials and Material Synthesis

The chemical reagents, e.g., nitric acid (HNO_3, A.R. grade), phosphoric acid (H_3PO_4, A.R. grade), 2-amino-2-hydroxymethyl-propane-1,3-diol (tris-base, A.R. grade), and chicken egg white ovalbumin (OVA, grade II), were

purchased from Sigma-Aldrich (USA). These were used without further purification. In the synthesis process, calcium oxide (CaO) was first synthesized from discarded egg shells (Rivera *et al.*, 1999). Briefly, the egg shells were cleaned with distilled water at 80 °C and dried *in vacuo*. They were then calcined at 1000 °C in a Lindberg LBF799C oven, in two heating stages (i. 25 to 700 °C for 2 h to eliminate organic substances and ii. 700 to 1000 °C for another 2 h to eliminate CO_2 to finally obtain CaO powder). Then, 2.5 g of the CaO powder was dissolved in 25 mL of 1 M HNO_3 under gentle stirring at 70 °C for 3 h. Subsequently, 3.0 g of conc. H_3PO_4 (85 wt.-%) was added dropwise into the solution to adjust the Ca/P ratio to 1.67. The pH of the mixed solution was maintained at 2.0 and the whole system was continuously stirred at room temperature. Precisely 2.0 g of OVA was then added into 500 mL of the obtained solution under vigorous stirring for 1 h. Precipitation was achieved after 200 mL of 1, 1.5, or 2 M tris-base had been added into the solution to impart the buffering effect to the solution at pH of 7, 8, or 9, respectively. The mixture was vigorously stirred. The precipitates were filtered, washed several times with deionized water, and lyophilized for 48 h. The procedure was repeated to obtain the precipitates that did not contained OVA for comparative purposes.

4.3.2 Characterization

A Rigaku D/MAX 2000 X-ray diffractometer (XRD) was used to investigate the crystalline nature of the obtained powdery precipitates, using Cu Kα (1.54 Å) radiation over the 2θ range of 5-60° with 0.02° scanning step. The crystalline phase of the powder was identified with JCPDS standard (9-432). A Nicolet NEXUS 670 Fourier-transform infrared spectroscope (FT-IR), operating at a resolution of 4 cm^{-1} over a wavenumber range of 4000 to 400 cm^{-1}, was used to examine the chemical functionalities of the powdery products. A Perkin-Elmer TGA-7 thermogravimetric analyzer (TGA) was used to investigate the thermal degradation behavior of the powder at a heating rate of 10 °C·min^{-1}. Microscopic morphology of the powder was observed by a JEOL JEM-2100 transmission electron microscope (TEM), operating at 200 kV. Surface morphology of the obtained products was investigated by a JEOL JSM-5410LV scanning electron microscope (SEM). Particle

size distribution of the powder was collected by a Mastersizer 2000 Malvern particle size analyzer (PSA). The powder was dispersed ultrasonically in water during the measurement. The pore characteristics and the Bruaauer-Emmett-Teller (BET) specific surface area of the obtained powdery products were determined based on the physi-sorption of N_2 at a temperature of 77 K using a Quantachrome AS-1 autosorb-1 instrument. Each experiment was performed in triplicate.

4.4 Results and Discussion

Due to the similarity of the results of the HAp particles that had been obtained at pH's 7, 8, and 9, only the results of the particles that had been obtained at pH 9 were extensively reported and discussed. As shown in Figure 4.1, all of the crystalline peaks as observed in the XRD patterns of the precipitated powdery products that had been obtained, both in the absence and the presence of OVA, at pH 9 could be assigned to those of HAp [i.e., the hexagonal P63/m space group with the lattice constants of $a = b = 0.9418$ nm and $c = 0.6884$ nm (cf. JCPDS No. 09-0432)]. The crystallite sizes, as estimated from the width of the (002) reflection peaks using the Scherrer's equation (Manafi *et al.*, 2008), were around 17.3-20.9 nm and 16.8-19.8 nm for the HAp and the HAp/OVA composite particles, respectively (see Table 4.1). Noticeably, the crystallite size decreased with an increase in the pH used during the precipitation process. As the pH increased, more tris-base molecules, in their free from, would be available to nucleate the HAp crystalline entities (cf. the pKa of tris-base = 8.06), hence the observed decrease in the crystallite size. At the same pH, the presence of OVA resulted in a slight reduction in the size of the obtained HAp crystals. This is because OVA influences aggregation to form primary particles, perhaps by adsorbing on the surface and changing interaction forces in suspension during the measurement of particle size in water or during the synthesis.

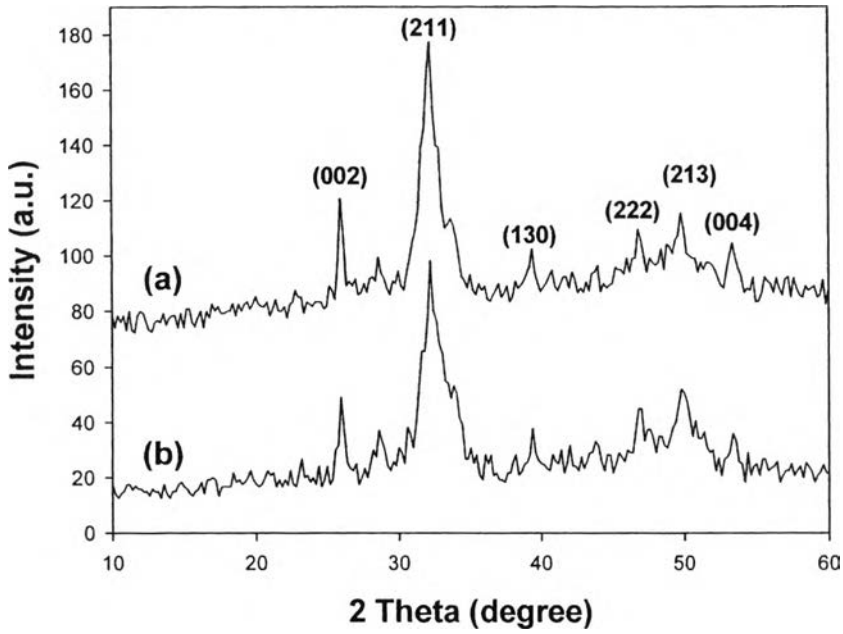

Figure 4.1 XRD patterns of (a) pure HAp and (b) HAp/OVA composite particles that had been obtained at pH 9.

Table 4.1 Textural parameters of pure HAp and HAp/OVA composite particles that had been obtained at different pH conditions

Type of HAp	Crystallite Size (nm)	Average Primary Size of Particles (nm)	BET Specific Surface Area ($m^2 \cdot g^{-1}$)	Pore Diameter (nm)	Pore Volume ($cm^3 \cdot g^{-1}$)
HAp (pH 7)	20.9	59.3	17.2	8.9	0.079
HAp (pH 8)	19.2	57.7	16.1	8.3	0.053
HAp (pH 9)	17.3	56.5	15.6	8.1	0.029
HAp/OVA (pH 7)	19.8	50.4	21.3	15.5	0.089
HAp/OVA (pH 8)	18.4	49.1	19.5	14.4	0.058
HAp/OVA (pH 9)	16.8	46.2	16.6	14.1	0.036

The FT-IR spectra of the HAp and the HAp/OVA composite particles that had been obtained at pH 9 as well as that of the as-received OVA in its dry state are shown in Figure 4.2. For the HAp particles, the adsorption bands centering at 3569 and 1630 cm^{-1} could be assigned to the OH stretching and the OH vibration of the apatitic group (Suwa *et al.*, 1993). The bands centering at 1035, 601, and 563 cm^{-1} should correspond to PO_4^{3-} ions in the HAp structure. However, the band centering at 1384 cm^{-1} was thought to belong to the carbonate functionality, which might be a result of the contamination from the reaction with CO_2 in the atmosphere (Wang *et al.*, 2006). As for the as-received OVA, the characteristic absorption peaks at 3299, 1652, 1539, and 1457 cm^{-1} could be ascribed to the N-H stretching vibration, the carbonyl vibration, the C-N vibration, and the C-H stretching vibration, respectively (Zhao *et al.*, 2008). For the HAp/OVA composite particles, the presence of the absorption bands centering at 1654 and 1539 cm^{-1} confirmed the presence of OVA within the obtained HAp particles.

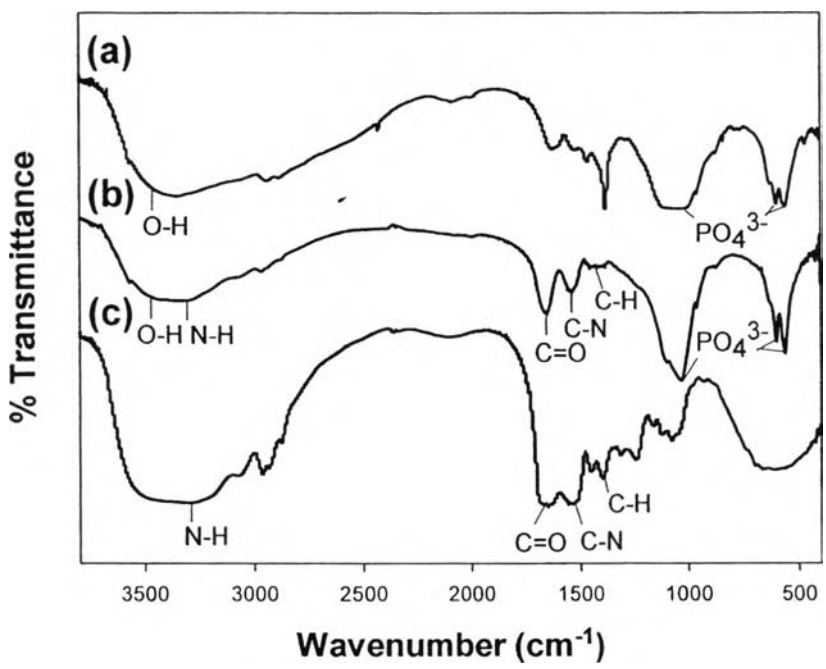

Figure 4.2 FT-IR spectra of (a) pure HAp and (b) HAp/OVA composite particles that had been obtained at pH 9 as well as that of (c) as-received OVA in its dry state.

The HAp and the HAp/OVA composite particles that had been obtained at pH 9 were evaluated thermogravimetrically and the results are shown in Figure 4.3. For the HAp particles, three stages in the loss of mass were observed. The first stage occurred over the temperature range of 60-160 °C, corresponding to the loss of adsorbed water. The second stage was observed at the onset temperature of about 240 °C. This should correspond to the loss of tris-base from HAp structure. The last stage was observed at the onset temperature of about 740 °C and this was thought to relate to the loss of the remaining organic residues within the HAp structure. As for the HAp/OVA composite particles, all of the three stages in the loss of the mass were also obtained, with an addition of another step being observed at the onset temperature of about 330 °C. This should correspond to the loss of the incorporated OVA. Apparently, both the FT-IR and the TGA results confirmed the presence of OVA within the structure of the obtained HAp/OVA composite particles.

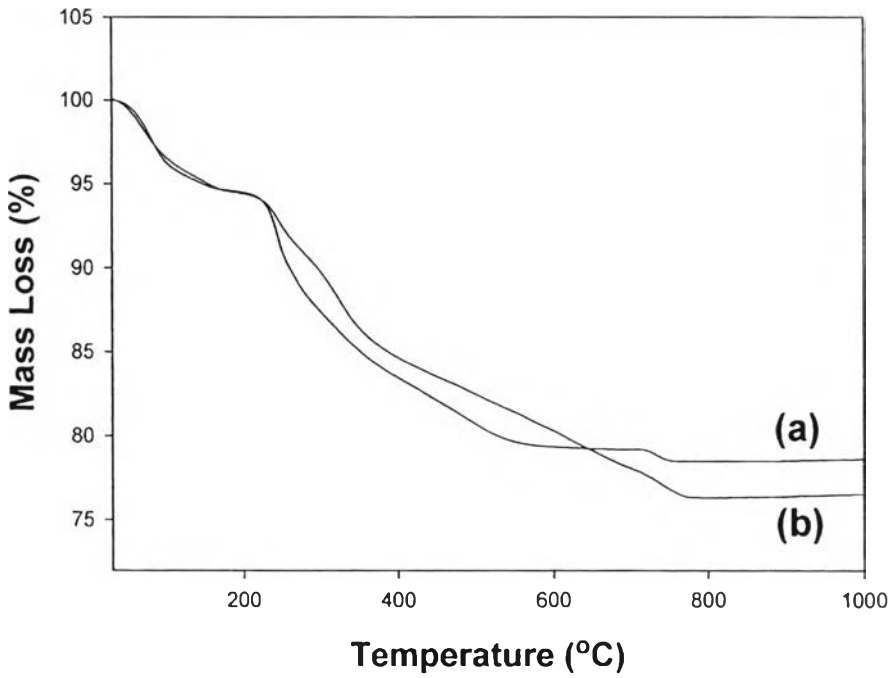

Figure 4.3 TGA curves of (a) pure HAp and (b) HAp/OVA composite particles that had been obtained at pH 9.

The particle size distribution (PSD) curves of the HAp and the HAp/OVA composite particles that had been obtained at pH 9 were presented in Figure 4.4. Based on PSD volume percentage, the HAp primary particles had the average sizes of around 56-59 nm and the HAp/OVA composite primary particles had the average sizes of around 46-50 nm. The average sizes of the HAp and the HAp/OVA composite primary particles that had been obtained at all pH's investigated were measured and summarized in Table 4.1. Apparently, the presence of OVA resulted in significant reduction in the size of the obtained HAp primary particles. On the contrary, the size was found to decrease slightly with an increase in the pH condition used during the precipitation process. Both of these should be a result of the increase in the number of nucleation sites, i.e., the presence of OVA in the former and the more availability of the free tris-base molecules in the latter (Chang *et al.*, 2003). As for the effect of tris-base, the greater the amount of tris-base used, the greater the number of nuclei, hence the observed reduction in the sizes of the HAp primary particles.

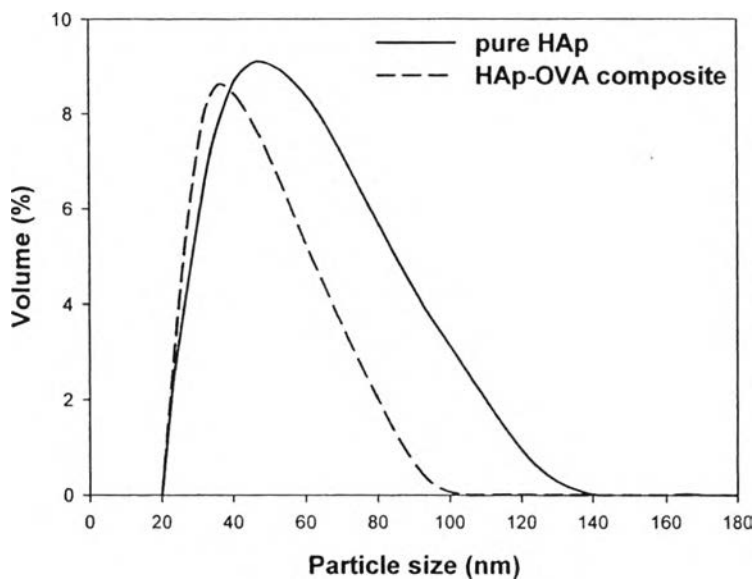

Figure 4.4 PSD curves of pure HAp and HAp/OVA composite particles that had been obtained at pH 9.

The nano-crystalline structure of the HAp and the HAp/OVA composite particles that had been obtained at pH 9 was investigated by TEM (see Figure 4.5). The rod-like morphology of the obtained HAp crystals, both in the absence and in the presence of OVA, was evident. The TEM result was consistent with the particle size distribution obtained using PSD, which revealed that the primary particles were in the nanometer range and the presence of OVA led to the reduction in the size of the primary particles. Despite the nano-crystalline nature of the individual primary particles, representative SEM images of the precipitated HAp and HAp/OVA composite powder that had been obtained at pH 9 (see Figure 4.6) revealed the agglomeration of them into large aggregates, the extent of which was accented by the presence of OVA. In addition, the HAp particles obtained at higher pH values existed as larger aggregates, owing possibly to the increase in the overall crystallization rate (viz. due to the increase in the nucleation rate, earlier mentioned) (Inskeep *et al.*, 1998).

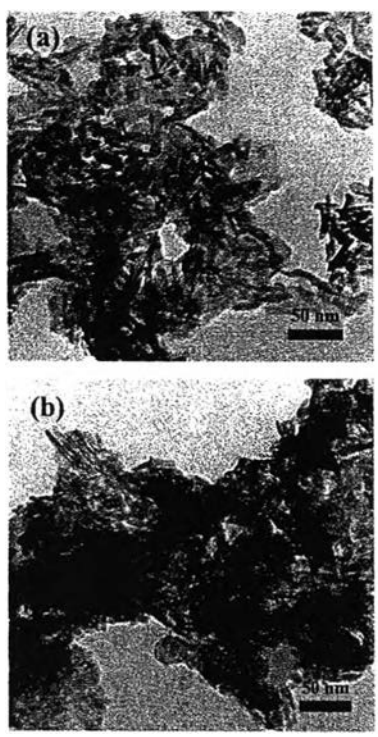

Figure 4.5 TEM micrographs of (a) pure HAp and (b) HAp/OVA composite particles that had been obtained at pH 9.

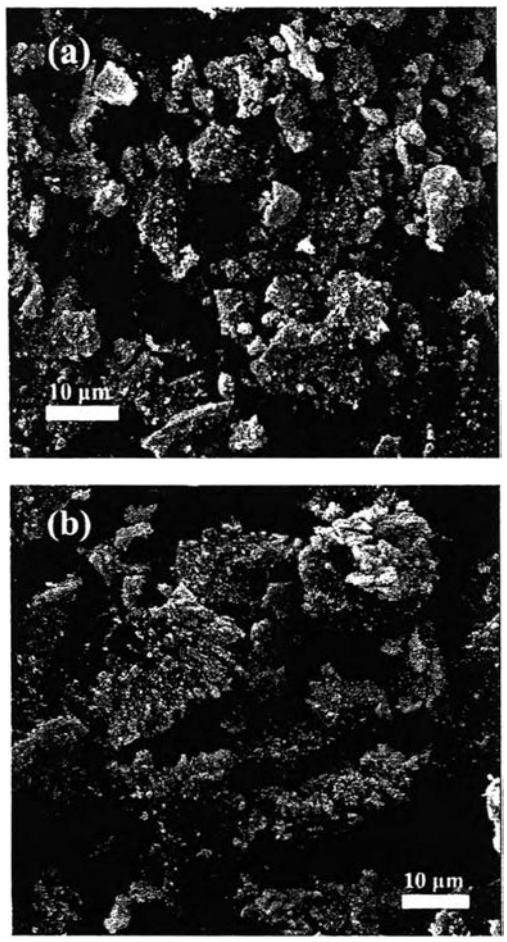

Figure 4.6 SEM images of (a) pure HAp and (b) HAp/OVA composite particles that had been obtained at pH 9.

The N_2 adsorption-desorption isotherms and the pore size distribution as calculated from the adsorption branch of the isotherms based on the Bopp-Jancsó-Heinzinger (BJH) model of the HAp and the HAp/OVA composite particles that had been synthesized at pH 9 are shown in Figure 4.7 and in the inset of the figure, respectively. The isotherms can be categorized as type IV, which can be further categorized into H1-hysteresis loops of mesoporous materials (Gregg and Sing, 1982) and the pore sizes of the HAp and the HAp/OVA particles were determined to be about 8.1 nm and 14.1 nm, respectively, on average. The isotherms and the pore size distribution of these two cases were slightly different. For the HAp/OVA

particles, the isotherm exhibited a slightly steeper slope with a greater pore volume and the pore size distribution was narrower, owing to the more uniform pore sizes. This indicates that the aggregation of OVA within the HAp structure affected slightly the basic pore structure of the obtained mesoporous HAp particles. The pore diameter and the BET specific average surface area for each of the obtained products are summarized in Table 4.1. In the absence of OVA within the HAp structure, the pore sizes were 8.1-8.9 nm. Larger pore sizes were observed for the OVA-incorporated HAp particles (i.e., 14.1-15.5 nm). These correspond to the BET specific average surface area values of 15.6-17.2 and 16.6-21.3 $m^2 \cdot g^{-1}$, respectively, and the pore volume values of 0.029-0.079 and 0.036-0.089 $cm^3 \cdot g^{-1}$, respectively. These pores were generated upon the sublimation of the as-formed ice crystals during the lyophilization step (Zhang, 2009; Yunoki, 2006). The presence of OVA resulted in hypothetical increases in the values of all of the pore parameters of the resulting HAp particles, while the increase in the pH during the precipitation process led to opposing trends. Furthermore, since the characteristic bands associated with both the HAp and OVA components in both the FT-IR and TGA profiles were not shifted, it is expected that the mesopores may be present as the voids located at the grain boundaries of the aggregates of the rod-like HAp particles.

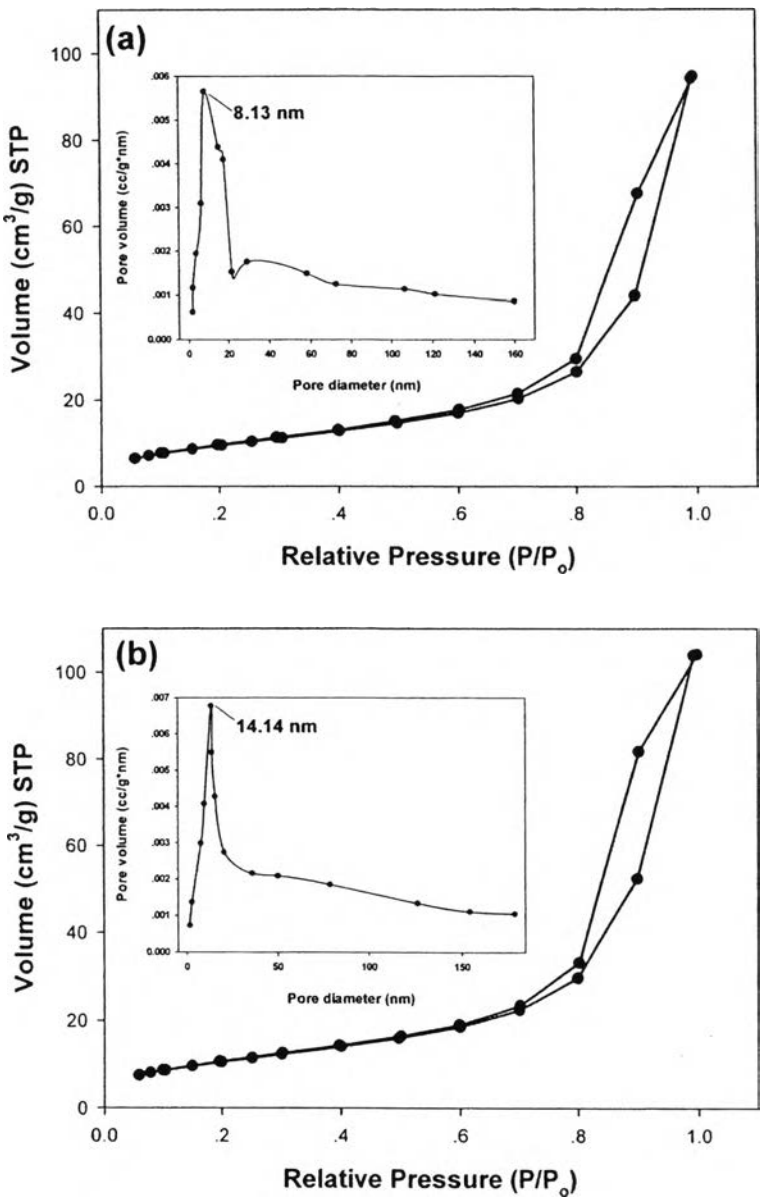

Figure 4.7 Adsorption-desorption isotherms of N_2 within the pore structures of (a) pure HAp and (b) HAp/OVA composite particles that had been obtained at pH 9. The size distribution of the pores as determined based on the Bopp-Jancsó- Heinzinger (BJH) model is shown as the inset.

4.5 Conclusions

An economical and simple synthetic route for HAp/OVA composite particles from discarded egg shells and OVA, as the model incorporating protein, by co-precipitation method was proposed. Both XRD and FT-IR results confirmed the formation of HAp, while PSD and TEM results indicated the formation of discrete HAp nanocrystals, which were rod- like in nature. Both the crystallite sizes (as calculated from breadth of the (002) reflection peak) and the sizes of the individual nanocrystalline particles decreased in the presence of OVA. However, the presence of OVA resulted in more agglomeration of the nanocrystalline particles, which had been proved by SEM analysis. The knowledge obtain from the preparation of these HAp/OVA composite materials could be used as a promising archetype for synthesizing composite particles of HAp and another functional protein for biomedical applications or bone tissue engineering purposes in particular.

4.6 Acknowledgments

The authors acknowledge the partial support received from 1) The Thailand Research Fund (TRF, grant no.: DBG5280015), 2) The Institute for the Promotion of Teaching Science and Technology (IPST, for the doctoral scholarship of P.K.), 3) The Petroleum and Petrochemical College (PPC), Chulalongkorn University, and 4) Center of Excellence on Petrochemical and Materials Technology (PETRO-MAT), Chulalongkorn University.

4.7 References

Bose, S. and Saha, S.K. (2003) Synthesis and characterization of hydroxyapatite nanopowders by emulsion technique. Chemistry of Materials, 15, 4464-4469.

Bose, S. and Saha, S.K. (2003) Synthesis of hydroxyapatite nanopowders via sucrose-templated sol-gel method Journal of the American Ceramic Society, 86, 1055-1057.

Chang, M.C., Ko, C.C., and Douglas, W.H. (2003) Preparation of hydroxyapatite-gelatin composite. Biomaterials, 24, 2853-2862.

Djošic, M.S., Mišković-Stankovic, V.B., Minlojic, S., Kacarevic, Z.M., Bibic, N., and Stojanovic, J. (2008) Electrochemical synthesis and characterization of hydroxyapatite powders. Materials Chemistry and Physics, 111, 137-142.

Fischer, E.M., Layrolle, P., Van Blitterswijk, C.A., and De Bruijn, J.D. (2003) Bone formation by mesenchymal progenitor cells cultured on dense and microporous hydroxyapatite particles. Tissue Engineering, 6, 1179-1188.

Gregg, S.J. and Sing, K.S.W. (1982) Adsorption, Surface area and Porosity. London: Academic Press.

Inskeep, W.P. and Silvertooth, J.C. (1998) Kinetics of hydroxyapatite precipitation at pH 7.4 to 8.4. Geochimica et Cosmochimica Acta, 52, 1883-1893.

Ioku, K. and Kamitakahara, M. (2009) Hydroxyapatite ceramics for medical application prepared by hydrothermal method. Phosphorus Research Bulletin, 23, 25-30.

Kuriakose, T.A., Kalkura, S.N., Palanichamy, M., Arivuoli, D., Dierks, K., Bocelli, G., and Betzel, C. (2004) Synthesis of stoichiometric nano crystalline hydroxyapatite by ethanol-based sol-gel technique at low temperature. Journal of Crystal Growth, 263, 517-523.

Li, Y.B., Tjandra, W., and Tam, K.C. (2008) Synthesis and characterization of nanoporous hydroxyapatite using cationic surfactant as templates. Materials Research Bulletin, 43, 2318-2326.

Manafi, S., Rahimipour, M.R., Yazdani, B., Sadrnezhaad, S.K., and Amin, M.H. (2008) Hydrothermal synthesis of aligned hydroxyapatite nanorods with ultra-high crystallinity. International Journal of Engineering. Transcations B: Applications, 21, 109-116.

Rivera, E.M., Araiza, M., Brostow, W., Castaño, V.M., Díaz-Estrada, J.R., Hernández, R., and Rodríguez, J.R. (1999) Synthesis of hydroxyapatite from egg shells. Materials Letters, 41, 128-134.

Shanthi, P.M.S.L., Mangalaraja, R.V., Uthirakumar, A.P., Velmathi, S., Balasubramanian, T., and Ashok, M. (2010) Synthesis and characterization

of porous shell-like nano hydroxyapatite using Cetrimide as template. Journal of Colloid and Interface Science, 350, 39-43.

Suwa, Y., Banno, H., Mizuno, M., and Saito, H. (1993) Synthesis of compositionally regulated hydroxyapatite from $Ca(OH)_2$ and H_3PO_4. Journal of the Ceramic Society of Japan, 101, 642-647.

Viswanath, B. and Ravishankar, N. (2008) Controlled synthesis of plated-shape hydroxyapatite and implications for the morphology of the apatite phase in bone. Biomaterials, 29, 4855-4863.

Wang, H., Zhai, L., Li, Y., and Shi, T. (2008) Preparation of irregular mesoporous hydroxyapatite. Materials Research Bulletin, 43, 1607-1614.

Wang, Y.J., Chen, J.D., Wei, K., Zhang, S.H., and Wang, X.D. (2006) Surfactant-assisted synthesis of hydroxyapatite particles. Materials Letters, 60, 3227-3231.

Wu, Y. and Bose, S. (2005) Nanocrystalline hydroxyapatite: micelle template synthesis and characterization. Langmuir, 21, 3232-3234.

Yunoki, S., Ikoma, T., Monkawa, A., Kikuchi, M., Sotome, S., Shinomiya, K., and Tanaka, J. (2006) Control of pure structure and mechanical property in hydroxyapatite/collagen composite using unidirectional ice growth. Materials Letters, 60, 999-1002.

Zhang, Y., Zuo, K.H., and Zeng, Y.P. (2009) Effect of gelatin addition on the microstructure of freeze-cast porous hydroxyapatite ceramics. Ceramics International, 35, 2151-2154.

Zhao, H.S., He, W., Wang, Y.J., Yue, Y.Z., Guo, X.G., Li, Z.M., Yan, S.P., Zhou, W.J., and Zhang, X.D. (2008) Biomineralization synthesis of mesoporous hydroxyapatite-calcium pyrophosphate polycrystal using ovalbumin as biosurfactant. Materials Chemistry and Physics, 111, 265-270.

Zhao, H.S., He, W., Wang, Y.J., Zhang, X.D., Li, Z.M., Yan, S.P., Zhou, W.J., and Wang, J.C. (2008) Biomineralization of large hydroxyapatite particles using ovalbumin as biosurfactant. Materials Letters, 62, 3603-3605.

Zhao, H.S., He, W., Wang, Y.J., Zhang, X.Z., Li, Z.M., Yan, S.P., and Zhou, W.J. (2008) Biomimetic synthesis and characterization of hydroxyapatite crystal

with low phase transformation temperature. Journal of Chemical and Engineering Data, 53, 2735-2738.

Zhau, Y.F. and Ma, J. (2005) Triblock copolymer templating synthesis of mesostructured hydroxyapatite. Microporous and Mesoporous Materials, 87, 110-117.